Handheld, Low-Cost, Aptamer-Based Sensing Device for Rapid SARS-CoV-2 RNA Detection Using Novelly Synthesized Gold Nanoparticles

S. C. G. Kiruba Daniel, Poojitha S. Pai, Hemanth Reddy Sabbella, Kumar Singh, Ambica Rangaiah, Shantala Gowdara Basawarajappa, and Chetan Singh Thakur, *Senior Member, IEEE*

***Abstract*—The development of a cost-efficient device to rapidly detect pandemic viruses is paramount. Hence, an innovative and scalable synthesis of metal nanoparticles followed by its usage for rapid detection of severe acute respiratory syndrome coronavirus-2 (SARS-CoV-2) has been reported in this work. The simple synthesis of metal nanoparticles utilizing tin as a solid-state reusable reducing agent is used for the SARS-CoV-2 ribonucleic acid (RNA) detection. Moreover, the solid-state reduction process occurs faster and leads to the enhanced formation of silver and gold nanoparticles (AuNPs) with voltage. By adding tin as a solid-state reducing agent with the precursor, the nanoparticles are formed within 30 s. This synthesis method can be easily scaled up for a commercially viable process to obtain different-sized metal nanoparticles. This is the first disclosure of the usage of tin as a reusable solid-state reducing agent for metal nanoparticle synthesis. An electronic device, consisting of AuNPs functionalized with a deoxyribonucleic acid (DNA)-based aptamer, can detect SARS-CoV-2 RNA in less than 5 min. With an increase in SARS-CoV-2 variants, such as Delta and Omicron, the detection device could be used for identifying the nucleic acids of the COVID-19 variants by modifying the aptamer sequence. The reported work overcomes the drawbacks of complex instrumentation, trained labor, and increased turnaround time.**

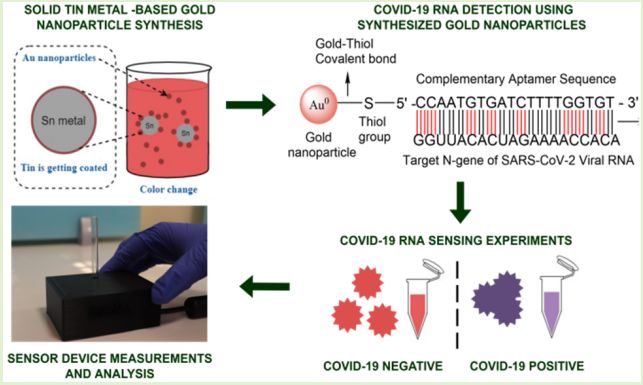

***Index Terms*—COVID-19, deoxyribonucleic acid (DNA) aptamer, electronic device, metal nanoparticles, severe acute respiratory syndrome coronavirus-2 (SARS-CoV-2) ribonucleic acid (RNA), solid-state reducing agent.**

Manuscript received 19 July 2022; revised 25 July 2022; accepted 29 July 2022. Date of publication 10 August 2022; date of current version 30 September 2022. This work was supported in part by the Science and Engineering Research Board (SERB)-National-Post Doctoral Fellow (N-PDF), Department of Science and Technology (DST), Government of India; and in part by the Scheme for Transformational and Advanced Research in Sciences, Ministry of Human Resource Development (STARS-MHRD), India. The associate editor coordinating the review of this article and approving it for publication was Prof. Chih-Ting Lin. *(S. C. G. Kiruba Daniel and Poojitha S. Pai contributed equally to this work.) (Corresponding author: S. C. G. Kiruba Daniel.)*

This work involved human subjects or animals in its research. Approval of all ethical and experimental procedures and protocols was granted in part by the Relevant Review Board and Ethics Committee of the Bangalore Medical College and Research Institute (BMCRI) under Approval No. BMCRI/PS/298/2020-21, 6 February 2021, and in part by the Institutional Human Ethics Committee of the Indian Institute of Science (IISc), 12 December 2021.

S. C. G. Kiruba Daniel, Poojitha S. Pai, Hemanth Reddy Sabbella, and Chetan Singh Thakur are with the NeuRonICS Lab, Department of Electronic Systems Engineering, Indian Institute of Science, Bengaluru 560012, India (e-mail: kirubadaniel@iisc.ac.in).

Kumar Singh, Ambica Rangaiah, and Shantala Gowdara Basawarajappa are with the Department of Microbiology, Bangalore Medical College and Research Institute, Bengaluru 560002, India.

This article has supplementary downloadable material available at https://doi.org/10.1109/JSEN.2022.3196598, provided by the authors.

Digital Object Identifier 10.1109/JSEN.2022.3196598

I. Introduction

IN DECEMBER 2019, a positive-strand ribonucleic acid (RNA) virus, severe acute respiratory syndrome coronavirus-2 (SARS-CoV-2), was identified as the causal agent of the ongoing COVID-19 pandemic, in Wuhan, China [1]. The prevalent symptoms that were observed in COVID-19 patients were fever, cough, sore throat, shortness of breath or dyspnea, and severe cases leading to pneumonia [2], [3]. The large-scale diagnosis of COVID-19 has been a major step in the identification of the infected population in a densely populated country, such as India, followed by the appropriate treatments, including medications and ventilator support, depending on the severity of the disease [4]. The current gold standard for accurately detecting SARS-CoV-2 RNA and diagnosing COVID-19 in any individual is real-time reverse transcriptase-polymerase chain reaction (RT-PCR), which involves detection and quantification of the viral RNA, if present, in biological specimens, including saliva, nasal, or throat swab of the individual [5], [6]. However, the disadvantages of this method are the time-consuming processes and the requirement of multiple steps with expensive equipment.

The cost involving diagnostic kits is also considered a significant drawback [7].

Aptamers, defined as short oligonucleotides composed of deoxyribonucleic acid (DNA) or RNA that bind to a specific target molecule, have recently gained attention in the area of biomolecule detection or biosensors. These oligonucleotides could be selected from a large nucleotide library of random sequences and allowed to interact as well as bind to target analytes of our interest via a process named systematic evolution of ligands by exponential enrichment (SELEX). This can be additionally termed *in vitro* selection or *in vitro* evolution. Antibodies have been utilized for the detection of various analytes, such as cortisol, alanine, and other biomolecules, but aptamers offer higher stability and longer shelf life at ambient conditions [8]–[10]. Also, aptamers are synthesized on large scale in a brief period of 2–3 h and, hence, could be used for rapid deployment during pandemics. For biological molecule detection, aptamers can be bound to nanoparticles synthesized from gold or silver precursors for easy and selective sensing of the target [11], [12]. Nanoparticles are scaled to a size of 1–100 nm in diameter and have a wide range of applications, including bio-sensing of analytes when conjugated with various biomolecules [13]. A solution of gold nanoparticles (AuNPs) functionalized with DNA-based aptamers is a simple technique to detect SARS-CoV-2 genes in a short time, since the aptamer can be applied to target a particular gene of the SARS-CoV-2 virus by complementary hybridization. Upon RNA–DNA hybridization, the solution shows a color change in response to the change in the surface properties of AuNPs [14], [15]. To date, AuNP synthesis required elevated temperature and reaction time, whereas the current method of nanoparticle synthesis using a solid-state metal reducing agent requires less time under ambient conditions [16]–[18]. Moreover, antibody-based detection kits require exceptionally low storage temperature, which hampers their deployment at remote locations, whereas aptamer-based kits can be utilized and stored at room temperature, making them easily viable in remote areas.

Biosensors involving nanoparticles-mediated colorimetric detection of analytes, such as viral nucleic acids using aptamer-conjugated AuNPs, can be conveniently applied in current diagnostic scenarios [19], [36], due to the instant visible reaction in the sole presence of target analytes or lack thereof [20]. This is because of their enhanced optical properties, such as surface plasmon resonance (SPR) [21]. The electrons in the conduction band in proximity to the AuNP surface start oscillating collectively with the electric field oscillations of the incident light, which is referred to as SPR. The surface plasmons of the AuNPs exhibit characteristic colors at specific wavelengths. The size of the nanoparticles is indicated by the direction of the SPR peak shift. As the SPR peak shifts to the right, toward the wavelengths ranging from 600 to 630 nm, the size of the AuNPs increases due to aggregated forms (20–25 nm in size) and displays a bluish-gray color. The SPR peak shifting toward the left, wavelengths ranging from 520 to 530 nm, indicates AuNPs in a colloidal form (7–15 nm in size) with a characteristic wine-red color [22], [23].

Moitra *et al.* [24] demonstrated the detection of SARS-CoV-2 nucleic acid using AuNPs capped with antisense oligonucleotides (ASO), which were targeted toward the N gene (nucleocapsid phosphoprotein) of the coronavirus. This method was used to detect viral loads with a limit of detection (LOD) of 0.18 ng/μL of RNA. Various methods for the detection of SARS-CoV-2 proteins and target genes have been summarized and compared with our method and electronic device in Table I. The three methods of detection, namely, the graphene-based DNA sensor [41], the electrochemical magnetoassay [31], and the saliva-based immunosensor [32], are presented with moderately high turnaround times, ranging from 30 min to 2 h, which could be unfavorable in the current scenario due to the need of rapid test results. Although the two methods, the label-free surface-enhanced Raman spectroscopy (SERS) biosensor [34] and the supersandwich electrochemical sensor [35], propose quick results

TABLE I
RECENTLY DEVELOPED RAPID COVID-19 DETECTION METHODS COMPARED WITH OUR METHOD AND DEVICE

COVID-19 Testing Methods	Sample used	Type of Sensor	Detection Limit	Analysis Time	Ref.
Graphene-based DNA Sensor	Complementary DNA sequence of SARS-CoV-2	Biotinylated ssDNA	100 fg/mL	<2 h	[41]
Electrochemical Magnetoassay	Saliva	Human ACE2 peptide	0.35 ag/mL	60 min	[31]
Saliva-based Immunosensor	Artificial saliva	Capture Antibody	3 pM	30 min	[32]
MIP-based Electrochemical sensor	Saliva	Molecularly imprinted polymer (MIP)	4.8 pg/mL	15 min	[33]
Label-free SERS Biosensor	Pseudoviruses samples	NaBH4 Silver nanoparticles	10 copies/test	2 min	[34]
Supersandwich Electrochemical sensor	Nasopharyngeal swabs	nCOVID-19 Antibody	200 copies/mL	10 s	[35]
Thermophotonic device	Clinical samples	Thermo-photonic LED	0.1 µg/mL	15 min	[40]
Handheld, Apta-AuNP based electronic sensor	**RNA from Nasopharyngeal Swabs**	**N-gene specific Aptamer based novel AuNPs**	**SARS-CoV-2 N gene Ct value of 25**	**<5 min**	**Current Method**

within seconds to minutes, the former method involves the usage of high-end machines for sample analysis using Raman spectroscopy, which cannot be used in remote areas for point of care applications. The latter, on the other hand, demands a time-consuming and laborious preparation of the graphene oxide-based nanocomposites requiring 30 h of synthesis, while our proposed method of tin metal-based AuNP synthesis allows the formation of nanoparticles within 30 s to 1 min. The novelty of our research work lies in the usage of a solid tin metal as a reducing agent for the formation of AuNPs from an auric chloride precursor within a minute, which has not been attempted previously to the best of our knowledge. Moreover, a SARS-CoV-2 gene-specific aptamer has been conjugated to the novelly synthesized AuNPs and applied to selectively detect the viral RNA in the clinical samples. Unlike the sample absorbance being measured over a broad wavelength range in standard plate readers, in our proposed method, the absorbance is measured only at two specific wavelengths using a 3-D-printed, handheld device employing two narrowband LEDs to rapidly distinguish COVID-19 clinical samples, thus lowering sensor readout time and power consumption. This portable, low-cost device can be utilized efficiently in a remote setting for point-of-care applications, replacing heavy, time-consuming, and sophisticated instruments.

Hence, our current research work proposes a low-power, low-footprint, and low-cost electronic sensing device for the rapid detection of SARS-CoV-2 RNA using novel AuNPs synthesized instantly with a solid, reusable tin metal as a reducing agent, presenting a cost-effective and energy-efficient choice over sensing devices with similar applications.

II. Materials and Methods

A. Materials

A gold chloride (III) hydrate of 500 gm (#MKCK6653) was purchased from Sigma-Aldrich Co., USA. Thiol-modified oligonucleotides with the selected sequence information (sequence 5'-CCAATGTGATCTTTTGGTGT-3') were synthesized and procured from Eurofins Genomics, Germany. A sodium chloride of 500 gm was purchased from Vasa Scientific Company (Bengaluru, India). The clinical viral RNA samples (SARS-CoV-2 and Dengue) were obtained from the Indian Council for Medical Research (ICMR)-approved Viral Research Diagnostic Laboratory (VRDL), Bangalore Medical College Research Institute (BMCRI), Bengaluru, after nucleic acid extraction using approved RNA extraction kits. The RNA extracts were obtained directly after the viral RNA extraction protocol was carried out by trained technicians at the BMCRI using the HiMedia viral RNA purification kit. The RNA samples have not been amplified or subjected to pretreatment using any techniques before the standard and sensor device measurements. The clinical samples have been randomly chosen with no specific criteria. All the experiments, including device testing and data acquisition, were carried out in the ICMR-approved State VRDL, BMCRI, Bengaluru, Karnataka. The institutional Ethical Committee Approval has been received from VRDL, BMCRI (No.: BMCRI/PS/298/2020-21), and the Indian Institute of Science (IISc) for the COVID-19 experiments performed in the study.

B. Synthesis and Characterization of Metal Nanoparticles Using a Metal Reducing Agent

Tin metal (0.4 g with a surface area of 670 mm^2) has been dipped into the aqueous precursor solutions of silver nitrate and auric chloride of 5-mM concentration. Other common metals, such as copper, aluminum, and lead, have not acted as reducing agents for the formation of silver and AuNPs, such as tin. A UV–Visible absorbance spectroscopy scan has been taken using a 96-well plate from 300 to 800 nm using a TECAN M200 Infinity Plate Reader. The formation of silver and AuNPs has been further confirmed by transmission electron microscopy (TEM), X-ray photoelectron spectroscopy (XPS), and X-ray diffraction (XRD) analysis. Analog discovery (AD) 2 (portable oscilloscope and waveform generator) is used for generating various signals using a waveform generator, ranging from 0 to 5 V. Jumper wires with bare copper wires coated with tin metal on the fringe are used as electrodes. A dc voltage sweep starting from 70 mV to 4 V on specific voltages is performed. Also, different ac waveform signals, sine, square, triangle, and trapezoidal, are given to silver nanoparticle and AuNP to observe the SPR behavior. After the nanoparticles are exposed to appropriate dc and ac voltages, the absorbance is measured using the TECAN M200 Infinity Plate Reader. Based on the experiments, a handheld prototype utilizing dc voltage having tin metal as an electrode as well as a solid-state reducing agent has been made.

C. Detection of SARS-CoV-2 RNA Using Metal Nanoparticles

AuNPs were selected for the detection of the SARS-CoV-2 RNA due to their robust sensing properties when conjugated with a specific complementary DNA sequence. The lyophilized aptamer was reconstituted with ultrapure Milli-Q water to prepare a stock concentration of 100 μM. From the aptamer stock solution, a final concentration of 5 μM was chosen for the experiments; 50 μL of the aptamer solution (5 μM) was added to 200 μL of synthesized AuNPs and allowed for conjugation for 30 min. The aptamer-functionalized AuNP mixture was incubated with viral RNA extracts (in the ratio of 4:3). A total of 15 samples, which includes 13 clinical samples and 3 control samples, were tested. Ten COVID-19 RNA samples, including five COVID-19 positive and five negative samples, and three Dengue RNA samples were used for the sensor measurements directly after viral RNA extraction and without further amplification or pretreatment. Three samples with ultrapure Milli-Q water and aptamer-functionalized AuNPs were used as controls for the experiment. A solution of sodium chloride (1M NaCl) was used as an aggregating agent to induce the AuNPs toward aggregation and produce an SPR change in the presence or absence of the SARS-CoV-2 nucleic acids. The absorbance values for thirteen samples were measured using the TECAN M200 Infinity Plate Reader and further tested in the sensor device. All the experiments were carried out at ideal conditions necessary for optimum sensing, at a temperature range of 25–27 °C and a neutral pH of 7.

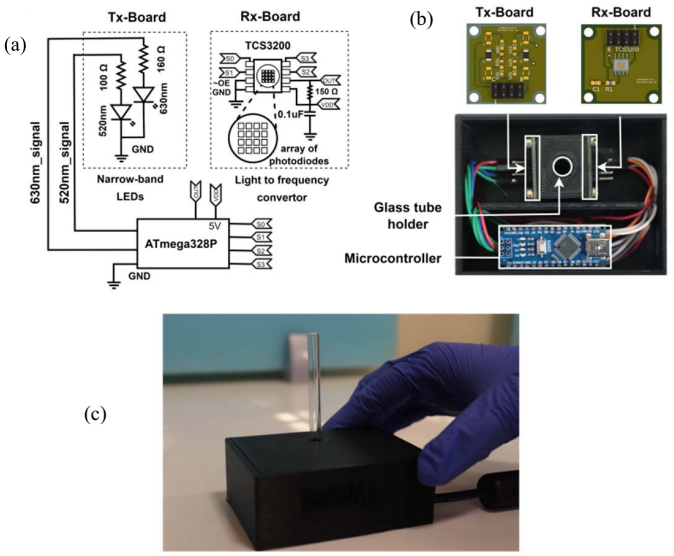

Fig. 1. Sensor setup. (a) Block diagram of the sensor setup. (b) Sensor prototype with Tx and Rx boards interfaced with the microcontroller and enclosed in a 3-D printed case. (c) Measurement setup in the 3-D printed sensor prototype.

D. Sensor Device Setup and Characterization

A low-cost, small form factor device has been built using the transmitter (Tx) and receiver (Rx) boards. The Tx board has narrowband, wavelength-specific, surface mount LEDs for 520- and 630-nm light with ±5-nm bandwidth. These LEDs are adjusted to have the same luminous intensity by selecting the appropriate current limiting resistor on the board. The Rx board has TCS3200, a light-to-frequency converter IC, which converts the irradiance proportional to the frequency of the output square wave. The output frequency scaling and the range of bandwidth in the IC can be configured using *S*0–*S*3. Both Tx board and Rx board are interfaced with a nano-microcontroller, and the corresponding frequency data are used to measure the absorbance of the analyte. The block diagram of the setup is shown in Fig. 1(a). The entire setup for mechanical design is 3-D modeled and printed for beamed light from the Tx board to pass through the glass cuvette and projected on the Rx board, as shown in Fig. 1(b). The complete sensor device costs less than 20 USD (≈1580 INR) and can further be priced at less than a USD (≈80 INR) per test. Signal calibration and conditioning techniques, such as zero referencing and range mapping, have been used to maintain the consistency of the readings. The readings are checked for the relative absorbance difference between the control and test samples.

The sensor device measurements are performed using a 5-mm test tube with a mixture of COVID-19 RNA samples and aptamer-functionalized AuNPs. The test tube is inserted into the glass tube holder, as shown in Fig. 1(c). The device checks the absorbance of the AuNPs in the test/control samples at two different and specific wavelengths, instead of a broad range of wavelength as conventionally measured in standard plate readers. These values are read from the TCS3200 chip by the microcontroller and sent to the serial monitor using a Universal Serial Bus (USB) cable. The sensor values are averaged over a fixed time interval to avoid any abrupt transitions and compared with the gold standard using the TECAN M200 Infinity Plate Reader.

III. Results and Discussion

A. Synthesis and Characterization of Metal Nanoparticles

Silver nanoparticle and AuNP formation has been observed by the color change in the solution from transparent to a yellowish color indicating the formation of silver nanoparticles and color change from transparent to a wine-red color indicating the formation of AuNPs. The narrow peak of SPR at 412 and 536 nm has been obtained for silver nanoparticle and AuNP, respectively, which correspond to their characteristic SPR peaks [25], [26]. There is a blueshift of the SPR peak of silver nanoparticles with increasing time from 30 s to 5 min, as shown in Fig. A.1.1 in the Supplementary Material. Characterization data of metal nanoparticles using XRD and TEM were also obtained in Fig. A.1.2 in the Supplementary Material. Also, an increase in the surface area of the tin metal led to the enhanced formation of silver nanoparticles with a slight blueshift in the SPR peak. Size variation is observed when increased exposure of tin metal to silver nitrate and auric chloride solution is done. Initially, at 30 s, bigger dendrite-like structures were observed, followed by around 15–18-nm size metal nanoparticles, followed by 7–9-nm size silver nanoparticle and AuNP. Fig. A.1.3 in the Supplementary Material shows that a decrease in nanoparticles size with increased exposure to a solid-state metal reducing agent might be due to the higher reduction potential of the reducing agent. XPS studies done on the surface of the solid-state metal reducing agent have revealed the presence of SnO, which is absent after the synthesis of silver nanoparticle and AuNP. Also, the presence of silver nanoparticle and AuNP has been established by the presence of Ag 3d and Au 4f peaks in the XPS spectra in Fig. A.1.4 in the Supplementary Material. Previously, the reduction potential of tin acetate as a reducing agent (in liquid form) for the non-aqueous synthesis of silver nanoparticles was reported in 2011 [27].

The impact of voltage on the synthesis of silver nanoparticles using tin metal as an electrode and as a solid-state reducing agent has been analyzed. There is a clear improvement in the formation of silver nanoparticles, which is evident from the SPR peaks. The impact of different voltages (50 mV–5 V) has been verified on auric chloride, and the formation of AuNPs and silver nanoparticles has been observed with increasing absorbance with increasing voltage. A frequency sweep of the sine wave from 1 kHz to 1 MHz is also done to observe the effects of frequency on the AuNPs. Different ac waveforms have also been performed by providing sine, square, triangle, and trapezoid waveforms, as represented in Fig. 2.

The plausible mechanism of the formation of nanoparticles in the presence of tin metal as a solid-state reducing agent has been schematically represented in Fig. 3. The tin metal reacts vigorously with precursor solution with high reducing potential and, hence, acts as a solid-state reducing agent. Earlier tin acetate in liquid form has been used as a reducing agent for the non-aqueous synthesis of metal nanoparticles where the reducing agent is lost during the synthesis reaction.

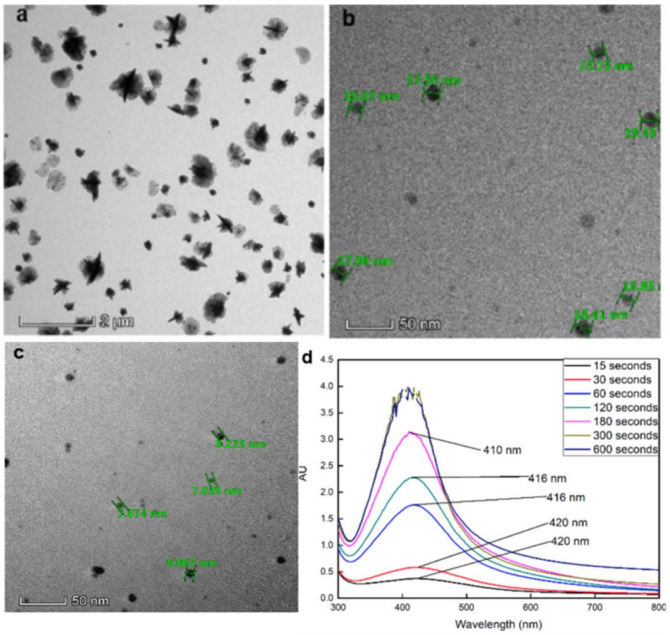

Fig. 2. (a)–(c) TEM image of silver nanoparticles and (d) UV–Vis absorbance graph plotted for silver nanoparticles synthesized with voltage applied with a solid-state metal reducing agent for various time durations.

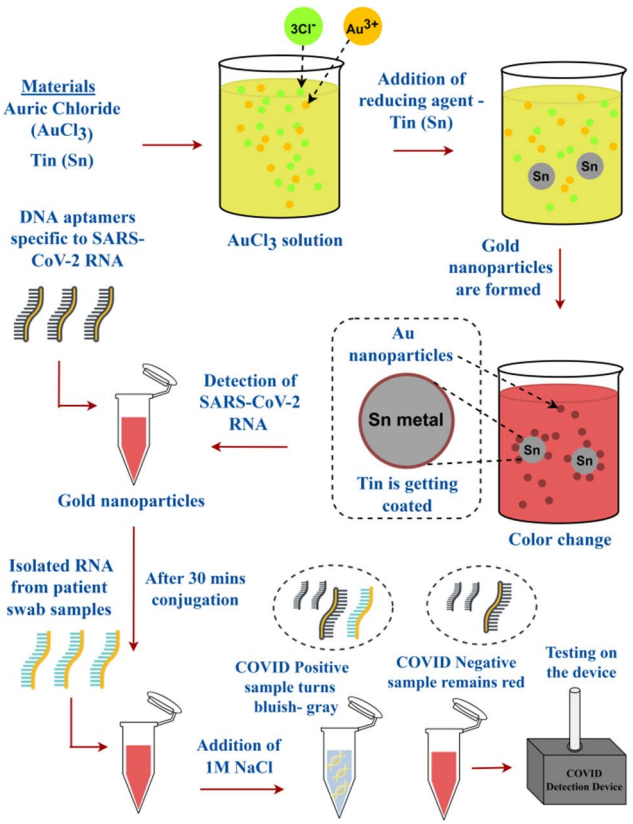

Fig. 3. Schematics of AuNP synthesis using a solid-state metal reducing agent and the detection of SARS-CoV-2 RNA with aptamer-functionalized AuNPs, followed by testing on an electronic sensing device.

But, in this current work, the solid-state reducing agent can be reused and has been demonstrated for aqueous controlled synthesis of metal nanoparticles. Herein, we report that the tin metal can be used several times without any significant loss of the metal during each synthesis reaction. The AuNPs synthesized with the tin metal reducing agent could be used for the detection of SARS-CoV-2 nucleic acids, making it a significant diagnostic tool for the ongoing pandemic. Initially, the synthesis of AuNPs is carried out using tin metal as a reducing agent added to the auric chloride solution. The nanoparticles are formed within 30 s to 2 min, indicated by the wine-red color of the solution. The newly synthesized AuNPs are applied for SARS-CoV-2 RNA detection in the RNA extracts from swab samples. The principle is based on the selective aggregation of AuNPs in the presence of SARS-CoV-2 RNA. The absorbance proportional to the SPR change in the solution can be sensitively measured and recorded by the portable electronic device in a real-time, clinical setting.

B. Detection of SARS-CoV-2 RNA Using Aptamer-Functionalized AuNPs

The AuNPs have been synthesized by reducing the precursor solution of auric chloride using solid tin metal as a reducing agent. This is visualized by the immediate color change of the precursor solution from a pale-yellow to a wine-red color, due to a change in the SPR of AuNPs. These AuNPs have been functionalized with a chemically synthesized aptamer attached to a thiol group (−SH) at the 5'-termini of the sequence. The aptamer sequence used in the experiments has been specifically chosen to target and bind to the nucleocapsid (N) gene of the SARS-CoV-2, due to the reduced sensitivity concerning the detection of the spike (S) gene in present diagnostic scenarios. The AuNP-aptamer conjugation is performed for 30 min until the thiol group attaches to the AuNP surface via a strong covalent bond. The SARS-CoV-2 RNA present in the samples, when mixed with the aptamer-functionalized AuNP solution, hybridizes to the complementary aptamer sequences, via double and triple hydrogen bonds, as per the Watson–Crick base pairing principle [28], [29].

The experimental results exhibit a change in the SPR of the AuNPs from a wine-red to a bluish-gray color for five COVID-19 positive clinical samples, whereas the solution remains a wine-red color for five COVID-19 negative samples due to the lack of an SPR shift. All samples containing SARS-CoV-2 RNA display a bluish-gray color due to the aggregation of AuNPs after the addition of sodium chloride, while all samples without SARS-CoV-2 RNA show no changes in the SPR, since there is the absence of AuNP aggregation. The reason for this observation is that the selective binding of the SARS-CoV-2 RNA to the sensing molecule, i.e., the RNA-specific aptamer, modifies the SPR of the AuNPs, followed by the addition of the sodium chloride, which induces changes in the refractive index of the metal–water interface, and produces a wavelength shift in the SPR peak in the COVID-19 positive samples, as shown in Fig. 4(a) and (b). However, the absence of binding events prevents the AuNPs from aggregation, even with the addition of sodium chloride in COVID-19 negative samples. Thus, the refractive index of the interface has not been affected and, hence, creates no shift in the SPR peak, as graphically represented in Fig. 4(c).

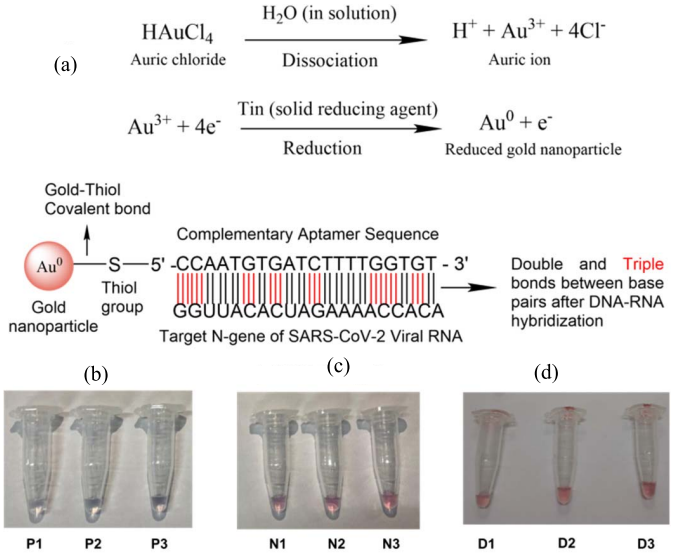

Fig. 4. Representative images showing an SPR change from a wine-red to a bluish-gray color in SARS-CoV-2 RNA positive samples. (a) Chemical reactions involved in the AuNP synthesis and chemical bonds involved in the interaction between SARS-CoV-2 RNA and aptamer-functionalized AuNPs. SARS-CoV-2 RNA samples detected using the specific aptamer sequence after RNA isolation showed a surface plasmon change only in (b) COVID-19 positive samples, but not observed in (c) COVID-19 negative samples as well as (d) Dengue positive samples.

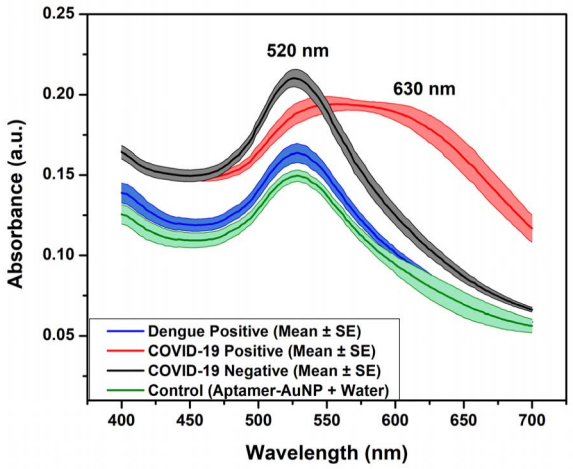

Fig. 5. Absorbance spectra taken using the TECAN M200 Infinity Plate Reader. Comparison of the SPR curve for the Dengue positive samples with the control sample (aptamer-functionalized AuNPs and water), COVID-19 positive and negative samples. The means and standard errors were calculated for five COVID-19 positives, five COVID-19 negatives, three Dengue positive samples, and three control samples.

C. Sensor Characterization

The absorbance spectra analyzed for the clinical samples using the TECAN M200 Infinity Plate Reader display a wavelength shift related to the SPR changes in the AuNPs based on whether they are aggregated or not. The readings show low absorbance values for the COVID-19 positive samples, which appear in a bluish-gray color due to the aggregated AuNPs and high absorbance values for the COVID-19 negative samples with a wine-red color due to unaggregated AuNPs at 520 nm wavelength (λ_{max}). In contrast, samples show relatively high absorbance for the COVID-19 positive samples and low absorbance for the COVID-19 negative samples at 630-nm wavelength (λ_{max}). The relative absorbance intensity at two specific wavelengths, 520 and 630 nm, after the wavelength shift, has been shown in Fig. 5 to differentiate the COVID-19 positive and negative samples.

The 13 clinical samples were tested in the device for relative absorbance for which the values were recorded, and graphs were plotted. The sensor outputs a frequency value directly proportional to the light intensity, which is inversely related to the absorbance of the sample. The SPR-related absorbance was significantly lower at the 520-nm wavelength for five COVID-19 positive samples and higher for five COVID-19 negative samples, which were consistent with the standard measurements in Fig. 5. On the other hand, the absorbance values recorded at 630 nm were relatively lower for the COVID-19 positive than the negative samples, as shown in Fig. 6(b). A simple and easy method of sample classification was identified to differentiate the COVID-19 positive samples from the COVID-19 negative and Dengue positive samples. The line joining the frequency readings at two wavelengths (520 and 630 nm), denoted as the slope, gives either a positive or negative slope. A positive slope is observed when one point at 520 nm ($p1$) is lesser than another point at 630 nm ($p2$). On the other hand, a negative slope is obtained when one point at 520 nm ($m1$ and $n1$) is greater than another point at 630 nm ($m2$ and $n2$). Our experimental results, represented in Fig. 6(a), show that the COVID-19 negative and Dengue-positive samples exhibit a negative slope ($m1 > m2$ and $n1 > n2$), while a positive slope ($p1 < p2$) is a characteristic feature of the COVID-19 positive samples.

D. Selectivity and Sensitivity of the Sensor

The selectivity of the aptamer to SARS-CoV-2 RNA was shown by selectivity experiments with RNA of other viruses, such as the Dengue virus (DENV), since its genetic material is also composed of positive-sense, single-stranded RNA. It has been observed that the results were similar to that of the COVID-negative samples, which confirms that the sensor is highly selective toward SARS-CoV-2 [30]. The device was able to differentiate the COVID-19 positive and negative samples at a moderately sensitive range, equivalent to the SARS-CoV-2 N gene Ct value of 25, corresponding to a medium viral load.

At present, the sensor device can address the COVID-19 samples having significantly lower cycle threshold (CT) values for the positive samples (CT $<$ 25) as well as detect higher CT values for the COVID-19 negative samples (CT $>$ 35). However, the CT values of the clinical samples that were detected using a standard viral quantification method are tabulated in Table A.2.1 in the Supplementary Material and correspond to the output frequency values measured in the sensor device. From Table A.2.1 in the Supplementary Material, a certain trend can be observed, correlating the standard CT values and sensor device frequency values, which may be used to determine the results for samples with CT values above 25 by

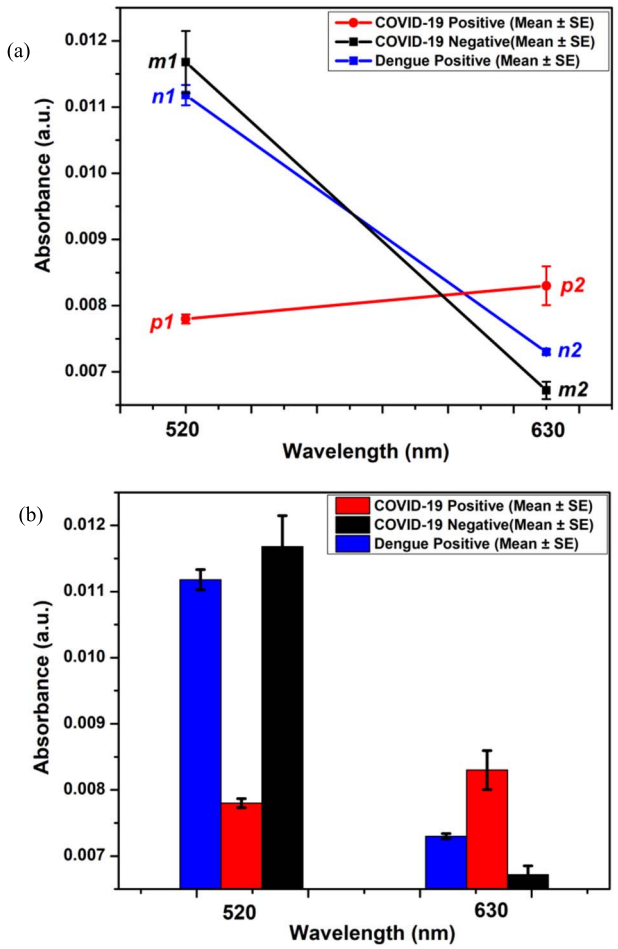

Fig. 6. Graphs with absorbance were plotted using values obtained from the sensor device after testing was performed on the device for the clinical samples. (a) Electronic device data shows a positive slope ($p1 < p2$) for the mean of five COVID-19 positive samples, while a negative slope ($m1 > m2$ and $n1 > n2$) is observed for the mean of five COVID-19 negatives and three Dengue positive samples. (b) Absorbance of the COVID-19 positive samples is higher than the COVID-19 negative and Dengue positive samples at the 630-nm wavelength, which is consistent with the wavelength shift in the COVID-19 positive samples. Lower absorbance for the COVID-19 positive samples at 520 nm is observed in comparison with the COVID-19 negative and Dengue positive samples.

establishing a baseline and extrapolating by the means of both extremes.

Triplicates were used to check the selectivity of the sensor device toward the COVID-19 RNA. The three clinical samples with DENV RNA showed no SPR shift, similar to that of the COVID-19 negative samples in Fig. 4(d). The SPR curve of the AuNPs present in the Dengue positive samples, measured using the TECAN M200 Infinity Plate Reader, was represented and compared with that of the control samples, COVID-19 negative and positive samples in Fig. 5, which was consistent with the device readings in Fig. 6. The SPR peak at 520 nm corresponds to high absorbance of the AuNPs, which is not aggregated in the Dengue positive samples, also observed for the control samples having only water with aptamer-functionalized AuNPs and COVID-19 negative samples. In contrast, the COVID-19 positive samples exhibit a low absorbance at 520 nm and have a high absorbance at

TABLE II
APTAMER ANALYSIS. THE DESIGNED APTAMER WAS ANALYZED BY THE OLIGOANALYZER TOOL TO UNDERSTAND ITS CHEMICAL PROPERTIES AND STRUCTURES

Aptamer Sequence	**5'- TATCACGCACTCGGTCTTCT –3'**
Target Gene Sequence	5'- AGAAGACCGAGTGCGTGATA - 3'
Length	20
GC Content	50%
Hairpin Structure	1
Maximum Delta G	-36.84 kcal/mole
Melt Temp	55.6 ºC
Molecular Weight	6018.9 G/Mole
Extinction Coefficient	177400 L/(Mole·Cm)
nmole/OD_{260}	5.64
µg/OD_{260}	33.93

630 nm owing to the SPR change in the aggregated AuNPs, which specifically absorbs light at 630 nm, in the presence of SARS-CoV-2 RNA. The presence of nucleic acids of the DENV, thus, does not influence the AuNP aggregation, in addition to the significant role played by the aptamer in the selective affinity toward the SARS-CoV-2 N gene. Hence, the aptamer was confirmed to exclusively hybridize to the RNA of the SARS-CoV-2 in the study.

The experiments in this study were carried out at 25–27 °C, since the temperature influences the chemical state and particle size of the AuNPs used, according to the previous literature [42], [43]. The AuNPs require specific temperatures and ideal particle size for optimum sensing of analytes, such as the viral RNA; therefore, the experiments were conducted at temperatures at which the AuNPs remain colloidal, smaller in size, and do not aggregate. This is because we need the aggregation of AuNPs to occur only after the addition of the viral RNA for observing visual and absorbance changes. Similarly, the functionalized aptamer also requires a prime temperature for conjugation to AuNPs as well as binding to the target RNA with maximum affinity [44]. Moreover, the viral RNA gets degraded at higher temperatures, making it unsuitable for detection and sensing. There is no observed influence of pH, since the sensing experiments involve testing on viral RNA extracted from clinical samples and are present in a buffer solution of constant pH [45]. Therefore, after considering all the abovementioned factors, the sensing reactions were carried out at a suitable temperature range (25–27 °C) and neutral pH (pH-7), without testing the effects of any variations in temperature or pH in the experimental study.

E. Aptamer Design and Sequence for SARS-CoV-2 Omicron Variant

Owing to the emergence of the newly identified SARS-CoV-2 Omicron variant, an attempt to design an aptamer targeting the spike mutations of the variant has been made. The nucleotide sequence of the surface spike glycoprotein (Locus: *GU280_gp02*, Protein ID: *YP009724390.1*, and GeneID:*43740568*) present in the Omicron variant (GenBank ID: OL *72836*) was searched in the National Center for Biotechnology Information (NCBI) GenBank database [36]

and aligned against the SARS-CoV-2 Delta variant (GenBank ID: *OK091006*) and the SARS-CoV-2 reference genome (Wuhan-Hu-1, *NC_04551*) using the NCBI-basic local alignment search tool (BLAST) [37]. The BLAST results showed a similarity of 98%, in which 3767 out of 3828 nucleotides were completely aligned, indicating a gap of 21 nucleotides. The nucleotide region showing consecutive gaps in the Delta–Omicron variant alignment was selected as the specific target for the aptamer sequence. The same nucleotide region showed gaps when the Omicron variant spike sequence was aligned with the spike sequence of the Wuhan-Hu-1 reference genome, as shown in Fig. A.1.5 in the Supplementary Material. The target sequence was then used as an input for a reverse complement tool [38], producing the final aptamer sequence that was 100% complementary to the target spike sequence of the Omicron variant. The final sequence was then analyzed by the OligoAnalyzer tool for theoretical values owing to its binding affinity and thermal stability, as described in Table II.

IV. Conclusion

A simple and low-cost electronic device to rapidly detect the SARS-CoV-2 genetic material (COVID-19) has been developed and tested with real-time samples. In addition, an easy and novel way to synthesize AuNPs using a solid-state reusable reducing agent, tin metal, has been reported, which can be scaled up and utilized for the detection of the SARS-CoV-2 (COVID-19) with the developed electronic device after conjugation with aptamers. The detection device along with the sensor has been both sensitive and selective to detect the SARS-CoV-2 nucleic acid, which is significant for the current COVID-19 outbreak. The slope joining the sensor readings at two different wavelengths has been identified as a simple classification method for COVID-19 clinical samples in the study. The developed electronic device cost would be less than 20 USD, and the cost per test would be less than a USD. Moreover, an aptamer sequence to detect emerging SARS-CoV-2 variants, such as Omicron, has been identified by a simple theoretical analysis, which can be utilized with AuNPs for new variant detection applications.

Acknowledgment

The authors would like to thank H. S. Nuthan for the support related to acquisition of clinical samples.

References

[1] J. Shang *et al.*, "Structural basis of receptor recognition by SARS-CoV-2," *Nature*, vol. 581, no. 7807, pp. 221–224, May 2020, doi: 10.1038/s41586-020-2179-y.

[2] C. Huang *et al.*, "Clinical features of patients infected with 2019 novel coronavirus in Wuhan, China," *Lancet*, vol. 395, pp. 497–506, May 2020. 10.1016/S0140-6736(20)30183-5.

[3] S. F. Pedersen and Y.-C. Ho, "SARS-CoV-2: A storm is raging," *J. Clin. Invest.*, vol. 130, no. 5, pp. 2202–2205, Apr. 2020, doi: 10.1172/JCI137647.

[4] T. Ji *et al.*, "Detection of COVID-19: A review of the current literature and future perspectives," *Biosensors Bioelectron.*, vol. 166, Oct. 2020, Art. no. 112455, doi: 10.1016/j.bios.2020.112455.

[5] Y. H. Baek *et al.*, "Development of a reverse transcription-loop-mediated isothermal amplification as a rapid early-detection method for novel SARS-CoV-2," *Emerg. Microbes Infections*, vol. 9, no. 1, pp. 998–1007, Jan. 2020, doi: 10.1080/22221751.2020.1756698.

[6] V. M. Corman *et al.*, "Detection of 2019 novel coronavirus (2019-nCoV) by real-time RT-PCR," *Eurosurveillance*, vol. 25, no. 3, Jan. 2020, Art. no. 2000045, doi: 10.2807/1560-7917.ES.2020.25.3.2000045.

[7] B. Udugama *et al.*, "Diagnosing COVID-19: The disease and tools for detection," *ACS Nano*, vol. 14, no. 4, pp. 3822–3835, Apr. 2020, doi: 10.1021/acsnano.0c02624.

[8] L. C. Bock, L. C. Griffin, J. A. Latham, E. H. Vermaas, and J. J. Toole, "Selection of single-stranded DNA molecules that bind and inhibit human thrombin," *Nature*, vol. 355, no. 6360, pp. 564–566, 1992, doi: 10.1038/355564a0.

[9] M. S. Soares *et al.*, "Label-free plasmonic immunosensor for cortisol detection in a D-shaped optical fiber," *Biomed. Opt. Exp.*, vol. 13, no. 6, pp. 3259–3274, 2022, doi: 10.1364/BOE.456253.

[10] A. K. Sharma and C. Marques, "Design and performance perspectives on fiber optic sensors with plasmonic nanostructures and gratings: A review," *IEEE Sensors J.*, vol. 19, no. 17, pp. 7168–7178, Sep. 2019, doi: 10.1109/JSEN.2019.2915274.

[11] S. C. G. K. Daniel, A. Kumar, K. Sivasakthi, and C. S. Thakur, "Handheld, low-cost electronic device for rapid, real-time fluorescence-based detection of Hg^{2+}, using aptamer-templated ZnO quantum dots," *Sens. Actuators B, Chem.*, vol. 290, pp. 73–78, Jul. 2019, doi: 10.1016/j.snb.2019.03.113.

[12] S. K. Daniel, L. A. N. Julius, and S. S. Gorthi, "Instantaneous detection of melamine by interference biosynthesis of silver nanoparticles," *Sens. Actuators B, Chem.*, vol. 238, pp. 641–650, Jan. 2017, doi: 10.1016/j.snb.2016.07.112.

[13] A. Belushkin, F. Yesilkoy, and H. Altug, "Nanoparticle-enhanced plasmonic biosensor for digital biomarker detection in a microarray," *ACS Nano*, vol. 12, no. 5, pp. 4453–4461, May 2018, doi: 10.1021/acsnano.8b00519.

[14] R. Elghanian, J. J. Storhoff, R. C. Mucic, R. L. Letsinger, and C. A. Mirkin, "Selective colorimetric detection of polynucleotides based on the distance-dependent optical properties of gold nanoparticles," *Science*, vol. 277, no. 5329, pp. 1078–1081, 1997, doi: 10.1126/science.277.5329.1078.

[15] J.-H. Lee *et al.*, "A novel rapid detection for SARS-CoV-2 spike 1 antigens using human angiotensin converting enzyme 2 (ACE2)," *Biosensors Bioelectron.*, vol. 171, Jan. 2021, Art. no. 112715, doi: 10.1016/j.bios.2020.112715.

[16] J. Turkevich, P. C. Stevenson, and J. Hillier, "A study of the nucleation and growth processes in the synthesis of colloidal gold," *Discuss. Faraday Soc.*, vol. 11, pp. 55–75, May 1951.

[17] G. Frens, "Controlled nucleation for the regulation of the particle size in monodisperse gold suspensions," *Nature Phys. Sci.*, vol. 241, pp. 20–22, Jan. 1973, doi: 10.1038/physci241020a0.

[18] J. Dong, P. L. Carpinone, G. Pyrgiotakis, P. Demokritou, and B. M. Moudgil, "Synthesis of precision gold nanoparticles using Turkevich method," *KONA Powder Part. J.*, vol. 37, pp. 224–232, Jan. 2020, doi: 10.14356/kona.2020011.

[19] P. Mehrotra, "Biosensors and their applications—A review," *J. Oral Biol. Craniofacial Res.*, vol. 6, no. 2, pp. 153–159, May 2016, doi: 10.1016/j.jobcr.2015.12.002.

[20] C. A. Mirkin, R. L. Letsinger, R. C. Mucic, and J. J. Storhoff, "A DNA-based method for rationally assembling nanoparticles into macroscopic materials," *Spherical Nucleic Acids*, vol. 382, pp. 3–11, Aug. 2020, doi: 10.4324/9780429200151-2.

[21] J. Polte *et al.*, "Mechanism of gold nanoparticle formation in the classical citrate synthesis method derived from coupled *in situ* XANES and SAXS evaluation," *J. Amer. Chem. Soc.*, vol. 132, no. 4, pp. 1296–1301, Feb. 2010, doi: 10.1021/ja906506j.

[22] C.-C. Huang, Y.-F. Huang, Z. Cao, W. Tan, and H.-T. Chang, "Aptamer-modified gold nanoparticles for colorimetric determination of platelet-derived growth factors and their receptors," *Anal. Chem.*, vol. 77, no. 17, pp. 5735–5741, Sep. 2005, doi: 10.1021/ac050957q.

[23] H. N. Daghestani and B. W. Day, "Theory and applications of surface plasmon resonance, resonant mirror, resonant waveguide grating, and dual polarization interferometry biosensors," *Sensors*, vol. 10, no. 11, pp. 9630–9646, Nov. 2010, doi: 10.3390/s101109630.

[24] P. Moitra, M. Alafeef, K. Dighe, M. B. Frieman, and D. Pan, "Selective naked-eye detection of SARS-CoV-2 mediated by n gene targeted antisense oligonucleotide capped plasmonic nanoparticles," *ACS Nano*, vol. 14, no. 6, pp. 7617–7627, Jun. 2020, doi: 10.1021/acsnano.0c03822.

[25] H. Granbohm, J. Larismaa, S. Ali, L.-S. Johansson, and S.-P. Hannula, "Control of the size of silver nanoparticles and release of silver in heat treated SiO_2–Ag composite powders," *Materials*, vol. 11, no. 1, p. 80, Jan. 2018, doi: 10.3390/ma11010080.

[26] Y. Q. He, S. P. Liu, L. Kong, and Z. F. Liu, "A study on the sizes and concentrations of gold nanoparticles by spectra of absorption, resonance Rayleigh scattering and resonance non-linear scattering," *Spectrochimica Acta A, Mol. Biomolecular Spectrosc.*, vol. 61, nos. 13–14, pp. 2861–2866, Oct. 2005, doi: 10.1016/j.saa.2004.10.035.
[27] R. Shankar, L. Groven, A. Amert, K. W. Whites, and J. J. Kellar, "Non-aqueous synthesis of silver nanoparticles using tin acetate as a reducing agent for the conductive ink formulation in printed electronics," *J. Mater. Chem.*, vol. 21, no. 29, pp. 10871–10877, 2011, doi: 10.1039/c0jm04521g.
[28] S. White, J. W. Szewczyk, J. M. Turner, E. E. Baird, and P. B. Dervan, "Recognition of the four Watson–Crick base pairs in the DNA minor groove by synthetic ligands," *Nature*, vol. 391, no. 6666, pp. 468–471, Jan. 1998.
[29] L. A. Marky, H. T. Lee, and A. Garcia, "Watson–Crick base Pairs and nucleic acids stability," Univ. Nebraska Med. Center, Omaha, NE, USA, Tech. Rep., 2010, doi: 10.1002/9780470015902.a0003126.pub2.
[30] L. Fabiani *et al.*, "Magnetic beads combined with carbon black-based screen-printed electrodes for COVID-19: A reliable and miniaturized electrochemical immunosensor for SARS-CoV-2 detection in saliva," *Biosensors Bioelectron.*, vol. 171, Jan. 2021, Art. no. 112686, doi: 10.1016/j.bios.2020.112686.
[31] E. D. Nascimento *et al.*, "COVID-19 diagnosis by SARS-CoV-2 spike protein detection in saliva using an ultrasensitive magneto-assay based on disposable electrochemical sensor," *Sens. Actuators B, Chem.*, vol. 353, Feb. 2022, Art. no. 131128, doi: 10.1016/j.snb.2021.131128.
[32] P.-H. Chen, C.-C. Huang, C.-C. Wu, P.-H. Chen, A. Tripathi, and Y.-L. Wang, "Saliva-based COVID-19 detection: A rapid antigen test of SARS-CoV-2 nucleocapsid protein using an electrical-double-layer gated field-effect transistor-based biosensing system," *Sens. Actuators B, Chem.*, vol. 357, Apr. 2022, Art. no. 131415, doi: 10.1016/j.snb.2022.131415.
[33] A. G. Ayankojo, R. Boroznjak, J. Reut, A. Öpik, and V. Syritski, "Molecularly imprinted polymer based electrochemical sensor for quantitative detection of SARS-CoV-2 spike protein," *Sens. Actuators B, Chem.*, vol. 353, Feb. 2022, Art. no. 131160, doi: 10.1016/j.snb.2021.131160.
[34] Z. Zhang *et al.*, "A novel enhanced substrate for label-free detection of SARS-CoV-2 based on surface-enhanced Raman scattering," *Sens. Actuators B, Chem.*, vol. 359, May 2022, Art. no. 131568, doi: 10.1016/j.snb.2022.131568.
[35] H. Zhao *et al.*, "Ultrasensitive supersandwich-type electrochemical sensor for SARS-CoV-2 from the infected COVID-19 patients using a smartphone," *Sens. Actuators B, Chem.*, vol. 327, Jan. 2021, Art. no. 128899, doi: 10.1016/j.snb.2020.128899.
[36] S. Sharma, S. Saini, M. Khangembam, and V. Singh, "Nanomaterials-based biosensors for COVID-19 detection—A review," *IEEE Sensors J.*, vol. 21, no. 5, pp. 5598–5611, Mar. 2021, doi: 10.1109/JSEN.2020.3036748.
[37] *NCBI GenBank Database*. Accessed: Feb. 3, 2022. [Online]. Available: https://www.ncbi.nlm.nih.gov/genbank/
[38] *NCBI-BLAST Tool*. Accessed: Feb. 3, 2022. [Online]. Available: https://blast.ncbi.nlm.nih.gov/Blast.cgi
[39] *Reverse Complement Tool*. Accessed: Feb. 3, 2022. [Online]. Available: https://www.bioinformatics.org/sms/rev_comp.html
[40] D. Thapa, N. Samadi, and N. Tabatabaei, "Handheld thermo-photonic device for rapid, low-cost, and on-site detection and quantification of anti-SARS-CoV-2 antibody," *IEEE Sensors J.*, vol. 21, no. 17, pp. 18504–18511, Sep. 2021, doi: 10.1109/JSEN.2021.3089016.
[41] S. Damiati *et al.*, "Flex printed circuit board implemented graphene-based DNA sensor for detection of SARS-CoV-2," *IEEE Sensors J.*, vol. 21, no. 12, pp. 13060–13067, Jun. 2021, doi: 10.1109/JSEN.2021.3068922.
[42] M. Tran, R. DePenning, M. Turner, and S. Padalkar, "Effect of citrate ratio and temperature on gold nanoparticle size and morphology," *Mater. Res. Exp.*, vol. 3, no. 10, Oct. 2016, Art. no. 105027, doi: 10.1088/2053-1591/3/10/105027.
[43] C. Li, D. Li, G. Wan, J. Xu, and W. Hou, "Facile synthesis of concentrated gold nanoparticles with low size-distribution in water: Temperature and pH controls," *Nanosc. Res. Lett.*, vol. 6, no. 1, pp. 1–10, Dec. 2011, doi: 10.1186/1556-276X-6-440.
[44] K. A. Peterlinz, R. M. Georgiadis, T. M. Herne, and M. J. Tarlov, "Observation of hybridization and dehybridization of thiol-tethered DNA using two-color surface plasmon resonance spectroscopy," *J. Amer. Chem. Soc.*, vol. 119, no. 14, pp. 3401–3402, Apr. 1997, doi: 10.1021/ja964326c.
[45] B. Contreras-Trigo *et al.*, "Slight pH fluctuations in the gold nanoparticle synthesis process influence the performance of the citrate reduction method," *Sensors*, vol. 18, no. 7, p. 2246, 2018, doi: 10.3390/s1807224.

S. C. G. Kiruba Daniel received the Ph.D. degree in nanotechnology from Anna University, Chennai, India, in 2015.

He was a Postdoctoral Researcher with the Instrumentation and Applied Physics Department, Indian Institute of Science (IISc), Bengaluru, India, where he is currently a Senior Research Associate with the NeuRonICS Lab, Department of Electronic Systems Engineering, under the guidance of Dr. Chetan Singh Thakur. He has authored or coauthored numerous research articles involving low-cost, nucleic acid-based, nanosensors for the detection of various analytes, such as melamine, heavy metals, proteins, and other biomolecules. His research interests include the development of low-cost and low-power nanotechnology-based sensing devices.

Dr. Kiruba Daniel was a recipient of the Gandhian Young Technology Innovator Award, whose expertise lies in solving environmental problems using nanotechnology.

Poojitha S. Pai received the M.Sc. degree in microbiology from Bangalore University, Bengaluru, India, in 2019.

She is currently a Project Associate with the NeuRonICS Lab, Department of Electronics Systems Engineering, Indian Institute of Science (IISc), Bengaluru. Her research interests include low cost, nucleic acid-based nanobiosensors for the detection of analytes, such as heavy metals, viral nucleic acids, venom toxins, and biomolecules.

Hemanth Reddy Sabbella received the B.Tech. degree in electronics and communication engineering from the Indraprastha Institute of Information Technology Delhi, New Delhi, India, in 2017.

He is currently a Project Associate with the NeuRonICS Lab, Department of Electronics Systems Engineering, Indian Institute of Science (IISc), Bengaluru, India. His research interests include VLSI design, embedded hardware, and electronic sensing devices.

Kumar Singh is currently a Research Scientist-B with the State Virus Research and Diagnostic Laboratory (VRDL), Bangalore Medical College and Research Institute (BMCRI), Bengaluru, India.

Ambica Rangaiah received the MBBS degree from Kuvempu University, Shivamogga, India, in 1998, and the M.D. degree in microbiology from the Rajiv Gandhi University of Health Sciences, Bengaluru, India, in 2002.

She is currently a Professor and the Head of the Department of Microbiology, Bangalore Medical College and Research Institute (BMCRI), Bengaluru. Her research interests include the development and evaluation of diagnostic kits related to COVID-19, Dengue, and other viral diseases.

Shantala Gowdara Basawarajappa received the MBBS degree from Bangalore University, Bengaluru, India, in 1994, and the M.D. degree in microbiology from the Rajiv Gandhi University of Health Sciences, Bengaluru, in 2000.

She is currently a Professor with the Department of Microbiology and a Principal Investigator with the State-Level Virus Research and Diagnostic Laboratory (VRDL), Bangalore Medical College and Research Institute (BMCRI), Bengaluru, India. She has authored or coauthored research articles related to the development, review, and evaluation of COVID-19, Influenza, and other viral diagnostic kits.

Chetan Singh Thakur (Senior Member, IEEE) received the Ph.D. degree in neuromorphic engineering from the MARCS Research Institute (Brain, Behavior, and Development), Western Sydney University, Penrith, NSW, Australia, in 2016.

He is currently an Assistant Professor with the NeuRonICS Lab, Department of Electronics Systems Engineering, Indian Institute of Science (IISc), Bengaluru, India. He is also an Adjunct Faculty with the International Centre for Neuromorphic Systems, Western Sydney University. His research interests include low-cost, low-power, brain-inspired intelligent machines, and electronics-integrated nanosensors.

Dr. Thakur was a recipient of the Young Investigator Award from the Pratiksha Trust, the Early Career Research Award by the Science and Engineering Research Board, India, and the Inspire Faculty Award by the Department of Science and Technology, India.